International Journal of Refractory Metals & Hard Materials 70 (2018) 124–133

Contents lists available at ScienceDirect

International Journal of Refractory Metals & Hard Materials

journal homepage: www.elsevier.com/locate/IJRMHM

Cold rolled tungsten (W) plates and foils: Evolution of the tensile properties and their indication towards deformation mechanisms

Simon Bonk[a,*], Jan Hoffmann[a], Andreas Hoffmann[b], Jens Reiser[a]

[a] Karlsruhe Institute of Technology, Institute for Applied Materials, 76344 Eggenstein-Leopoldshafen, Germany
[b] PLANSEE SE, 6600 Reutte, Austria

ARTICLE INFO

Keywords:
Ultrafine grained (UFG) tungsten
Tensile ductility
Screw dislocations
Deformation mechanisms
Dislocation-grain boundary interactions
Uniform elongation

ABSTRACT

This paper is the second part of our series on ultrafine-grained (UFG) tungsten produced by cold rolling. The aim of this paper is to determine tensile properties, with a focus on uniform elongation and flow stress, and to identify the mechanism of plastic deformation in cold rolled tungsten plates and foils. For this purpose, five plates have been rolled out of a single sintered compact with increasing degrees of deformation, which enables the analysis of mechanical properties with changing microstructure without influence from the chemical composition.

Uniaxial tensile tests have been performed in the range of room temperature to 800 °C. The tensile curves show a clear trend of increased strength for finer microstructures and simultaneously evolving room temperature ductility in the low temperature regime for cold rolled plates. The thinnest foil (100 µm) behaves uniquely by forming a plateau in the stress-strain curve, which hints at a change in the deformation mechanism.

Analyzing the temperature and grain size dependence of the flow stress reveals that the bulk plasticity is still controlled by screw dislocations and further suggests a change in the dislocation-grain boundary interactions from blocking at low homologous temperatures to absorbing at elevated temperatures.

A fracture analysis of cold rolled tungsten foils confirms a plastic deformation prior to fracture and reveals a steady transition from brittle towards lamellar fracture for the highly deformed tungsten foils.

1. Introduction

Technical pure tungsten is known for its outstanding thermophysical and thermochemical properties at high temperatures, provided that the work environment is oxygen-free. The highest melting point of all metals renders tungsten thermally stable against recrystallization at high working temperatures even as fine-grained material.

However, the technical application as structural material in high-temperature applications demands the assembly at room temperature, at which the brittle character of conventional tungsten prevents its application. Many efforts have been made to enhance the three main mechanical properties at room temperature: strength, ductility and toughness. An improvement can be achieved by alloying [1–3] or forming tungsten composites [4,5]. This however leads to a loss of the character of pure tungsten. A third approach which allows the application of single-phase, pure tungsten is tailoring the microstructure down to an ultrafine grain size by severe plastic deformation (SPD) as reviewed by Valiev et al. [6]. Many efforts have been made in this direction: equal channel angular pressing (ECAP) [7,8], high pressure torsion (HPT) [9,10] or heavily cold rolling (rolling well below the recrystallization temperature) [11–13]. The described decrease in grain size of a material by plastic deformation is known to increases the strength significantly, following the Hall-Petch relation [14,15]. This increase in strength is usually accompanied by a decrease in ductility (i.e. uniform elongation). Valiev et al. [16] could show that the unique microstructure of several SPD processed material leads to a paradoxon of increased strength and ductility. The SPD method can also be applied on commercial pure tungsten to refine the grain size into the ultrafine-grained (UFG) regime [17,18]. While evaluating such pure tungsten with a UFG microstructure for high-temperature applications, three paradoxes have been discovered, contradicting the expected behaviour going along the largely enhanced strength of UFG tungsten:

(1) an increased room-temperature toughness (K_{IQ}: e.g. L-T crack system 120 MPa($m^{0.5}$) [19,20],
(2) a decreased brittle-to-ductile transition temperature (BDTT) [21,22], and.
(3) an increased room-temperature tensile ductility [11].

* Corresponding author at: Karlsruhe Institute of Technology (KIT), Institute for Applied Materials (IAM-AWP), Hermann-von-Helmholtz-Platz 1, 76344 Eggenstein-Leopoldshafen, Germany.
E-mail address: simon.bonk@kit.edu (S. Bonk).

http://dx.doi.org/10.1016/j.ijrmhm.2017.09.007
Received 28 July 2017; Received in revised form 8 September 2017; Accepted 19 September 2017
Available online 21 September 2017

Based on these intriguing results, a more in-depth analysis of the evolution of these properties with decreasing grain size, from coarse grained to ultrafine grained, was initiated. This paper comprises the investigation of the tensile ductility by uniaxial tensile tests. Here, we define "ductility" as the uniform elongation (ε_{ue}), which, in contrast to the elongation at fracture (ε_{ef}), is independent of the sample thickness (t) and is, therefore, the technologically more relevant parameter ($\varepsilon_{ue} \neq f(t)$, $\varepsilon_{ef} = f(t)$) [23].

Plastic deformation in tungsten, as a model body centered cubic (bcc) material, was investigated quite thoroughly since the 1960s for single crystalline tungsten. Argon and Maloof [24] reported asymmetries in the critical resolved shear stress of operating slip planes, which suggests a failure of Schmid's Law at low temperatures [25]. Vitek [26,27] explained how the model of a screw dislocation crossing between energetically similar {110} and {112} planes depends on the orientation of the slip planes relative to the maximum resolved shear stress. He further showed that these screw dislocations account for the strong temperature dependence of flow stress below the critical temperature (T_c) observed in bcc materials. Atomistically, the temperature dependence can be understood by picturing a nonplanar dislocation core of the screw dislocation, which originates from the three-fold symmetric axis of the bcc structure [28]. This renders the dislocation difficult to displace, which is expressed through its high Peierls potential. However, the movement of the screw dislocations can be supported by thermal activation. Sesták and Seeger [29] postulated a double kink pair mechanisms, which enables the dislocation to overcome the Peierls barrier more easily by first dislocating a small part of the screw dislocation to the next energetic minima. This forms two edge dislocations between the old and the new screw dislocations. If these edge dislocations, called kinks, are formed with a sufficient minimal distance, they are then driven apart by the external force more easily than the screw dislocations due to their planar core. As a result, they move the whole screw dislocation to the next Peierls valley. This thermally activated process of kink formation explains the eased movement of screw dislocations with increasing temperature and the strain rate dependence of the flow stress below the critical temperature in bcc metals.

Even though the deformation mechanisms controlling the plastic deformation in a perfect (single) crystal of bcc material were thoroughly investigated, the influence of crystal defects (i.e. vacancies, dislocations and grain boundaries) on these deformation mechanisms is far less understood. To shed light on the influence of the microstructure on the mechanical properties and deformation mechanisms, tungsten with the same chemical composition must be investigated at consecutive steps of grain refinement. The authors showed this in the first paper of this series [30], where an increased degree of deformation, which was achieved through successive steps of cold rolling, led to a steady decrease in grain size into the ultrafine-grained regime. As a first benchmark regarding mechanical properties, it was shown that the hardness at room temperature of this cold rolled UFG tungsten matches the values of UFG tungsten produced by a similar procedure found in literature [11].

In this paper, a batch of technical pure tungsten sheets covering grain sizes from around 740 nm to 240 nm (UFG), as well as coarse-grained reference materials, should allow the investigation of mechanical properties at the transition from coarse-grained to UFG tungsten. To access important characteristic material properties, such as uniform elongation, flow stress and the ultimate tensile strength (UTS), the established technique of uniaxial tensile tests was employed. Tensile test results published in literature for single crystalline, recrystallized coarse-grained and hot rolled tungsten are compiled in Fig. 1, which shows the flow stress plotted against the testing temperature.

The following sections will address these questions:

(1) How do the (ultra)fine-grained foils respond to a tensile load at different temperatures in comparison to reference tungsten sheets?

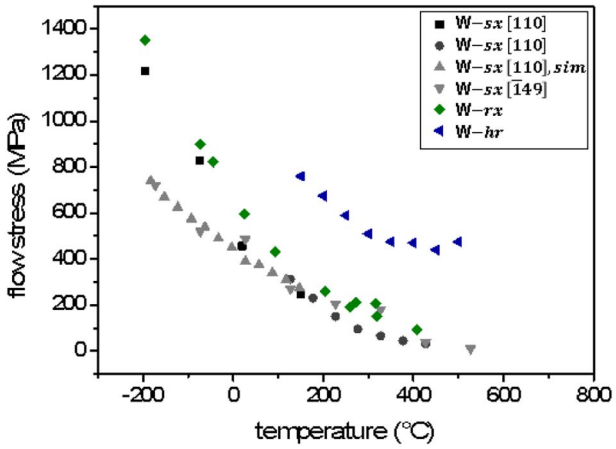

Fig. 1. Flow stress plotted against the testing temperature from tensile tests on tungsten single crystals (W-sx) [24,31,32], recrystallized coarse-grained material (W-rx) [3] and hot rolled tungsten (W-hr) [33], as well as results from simulated single crystalline tensile tests [34].

(2) How do the uniform elongation and flow stress change with increasing temperature and an increasing degree of deformation?
(3) What kind of fracture occurs for the different materials at different temperatures?
(4) Which indications towards deformation mechanisms can be inferred from the obtained results?

To address these questions, the paper is organised as follows: the microstructure of the tested cold rolled tungsten sheets, as well as of the reference materials, are described and compared regarding the main structural parameters, which is followed by a brief description of the experimental setup and the methods of evaluation. The tensile tests are evaluated regarding the curve shape and the associated hardening coefficients. Furthermore, the two main parameters for ductility – namely the uniform elongation and flow stress – are discussed regarding their dependence on temperature and their degree of deformation (grain size). Afterwards, the fracture surfaces are examined by electron microscopy (SEM). Finally, the observed trends in the tensile properties and fracture behaviour hint at the active deformation mechanisms, which are discussed.

2. Material and methods

2.1. Material

The microstructural analysis of the cold rolled tungsten used in this paper is described in detail in the first paper of this series [30]. The batch of samples was produced by PLANSEE SE in Reutte, Austria and consists of tungsten foils rolled out of a single sintered compact of technical pure tungsten (metallic purity > 99.97 wt% W) to five different thicknesses: 1 mm, 500 µm, 300 µm, 200 µm and 100 µm, which represents five different degrees of deformation. The use of a single sintered compact allows reducing the discussion of the mechanical properties to the microstructural influence, as the chemical composition is the same for all the sheets.

As reference materials, hot rolled tungsten (W-hr), recrystallized tungsten (W-rx) and a sintered compact of technical pure tungsten (W-si) are included in the mechanical testing campaign. For the recrystallized specimen, 1 mm cold rolled tungsten plates were annealed for 1 h at 2000 °C in a hydrogen oven (at PLANSEE SE). The microstructural analysis of the reference materials can be found in Ref. [21] for the recrystallized tungsten and in Ref. [35] for the hot rolled tungsten and the sintered compact.

All tested materials are summarised in Table 1, which includes their

Table 1
Overview of the tested materials, nomenclature and the most important structural parameters. The table contains data for five cold rolled tungsten sheets with increasing equivalent strain corresponding to a decrease in thickness from 1000 µm (W1000) to 100 µm (W100), as well as three reference materials: sintered tungsten (W-si), hot rolled tungsten (W-hr) and recrystallized tungsten (W-rx).

	Nomenclature	Material processing[a]	Specimen thickness (t)	Eq. strain[b]	Grain size (mean, S-Dir)	Hardness
			[µm]		[µm]	HV0.1
Cold rolled plates	W1000	si + hr + cr	1000	1.7	0.73	595
	W500	si + hr + cr	500	2.4	0.52	602
	W300	si + hr + cr	300	2.91	0.46	619
	W200	si + hr + cr	200	3.31	0.36	648
	W100	si + hr + cr	100	4	0.24	687
Reference	W-si	si	1000	–	10.7	370
	W-hr	si + hr	500	–	3.45	520
	W-rx	si + hr + cr + recrystallized[c]	1000	–	130	411

[a] Material processing: sintered (si), hot rolled (hr), cold rolled (cr).
[b] Equivalent strain is related to the dimension obtained after hot rolling.
[c] Recrystallized: 1 h, 2000 °C, in hydrogen.

nomenclature and their most important parameters. These specimens cover an average grain size that ranges from 130 to 3.45 µm, for the reference materials, to 730 nm (1 mm plate) and 240 nm (100 µm foil) for the cold rolled plates, which reaches well into the ultrafine-grain regime. The ultrafine-grain size in the cold rolled plates can be found perpendicular to the rolling direction, with the grains being taller in the other two directions. This results in “pancake” shaped grains. Further, the microstructural analysis revealed a pronounced α- and γ-fibre texture, where the highest intensities corresponded to the rotated cube component ((001) ⟨110⟩). This texture gets more and more pronounced with higher degrees of deformation. The grain refinement and the evolution of the texture comes with an increased number of high angle grain boundaries (HAGBs), while low angle grain boundaries (LAGBs) show no correlation with the degree of deformation introduced by cold rolling.

2.2. Tensile tests

Tensile tests, which were performed with a universal testing machine, are an established technique for determining characteristic material properties, such as uniform elongation, flow stress and the ultimate tensile strength. Especially the uniform elongation and the flow stress, the onset stress for plastic deformation, are of importance when discussing ductility in materials. The tensile tests further build the basis for the planned strain rate jump experiments, where the range of the elastic behaviour, the ultimate tensile strength and the range of uniform plastic deformation must be known.

The universal testing machine is an electro-mechanical, screw-driven Zwick Z100 with a 50 kN load cell and a vacuum oven surrounding the pull rods. To test our thin foils (as thin as 100 µm) at different temperatures ranging from 20 °C to 800 °C, a special holder had to be designed, which heats the samples before testing without preloading or bending the foils. It further enables the use of an extensometer to measure the elongation on the sample, which guarantees precise strain measurements. All tensile tests were performed displacement controlled, with a constant crosshead velocity of 0.015 mm/s, representing. This represents a strain rate of 10^{-3} l/s.

From the cold rolled tungsten sheets, the tensile test samples were cut as flat, bone-shaped specimens using wire-cut, electrical discharge machining. The surfaces of the samples were in their as-rolled and in their as-cut condition respectively, i.e. the sample surfaces were not polished after the rolling/cutting was performed. The gauge length measured 13 mm and the sample width 2 mm. The sample thickness corresponded to the thickness of the respective plate. All samples cut from the rolled specimen were retrieved in line with the rolling direction, so that the tensile direction lies parallel to the rolling direction.

3. Results

3.1. Tensile curves

Using the setup described in Section 2.2, it is possible to test, under the same conditions, all the different cold rolled foils (1 mm to 100 µm), as well as the three reference materials with coarser grain sizes: hot rolled tungsten (W-hr), recrystallized tungsten (W-rx) and a sintered compact of commercial pure tungsten (W-si). The resulting engineering stress-strain curves are plotted for the cold rolled plates in Fig. 2 and for the reference materials in Fig. 3. The tests cover a temperature range from 20 °C to 800 °C. Because all the reference materials showed brittle fractures between 200 °C and 300 °C, tests at lower temperatures were omitted.

Upon comparing the reference materials (Fig. 3), the recrystallized tungsten (b), as the coarsest material exhibited the lowest strength followed by the sintered compact (a). Both materials showed high elongation at fracture occurring above 350 °C, but they also showed pure brittle fractures at 300 °C and below. This fits the picture of a critical temperature in tungsten, below which, the screw dislocations impede plastic flow and, above which, they become fully thermally activated. The hot rolled tungsten (c), in comparison, exhibits stresses around three times higher and still shows plastic flow at 300 °C. However, at high temperatures, the hot rolled tungsten loses a significant amount of uniform elongation and elongation at fracture. The increase in strength and the loss of ductility can be easily traced back to the smaller grain size (see Table 1) and the rolling-induced lattice defects.

The tensile curves for the cold rolled plates (Fig. 2) reached significantly higher stresses than those reached by the reference materials (Fig. 3) and, at the same time, they showed room temperature ductility. However, the trend of reduced high-temperature ductility with increased rolling, as was already observed for the hot rolled material, continued for the cold rolled plates and foils.

Comparing the cold rolled tungsten plates to each other, the curve shapes for the 100 µm foil are striking: at room temperature, they show a nearly textbook-like, elastic-perfectly-plastic behaviour with a very narrow hardening region. At room temperature, the 100 µm foil (W100) reached a UTS of about 2300 MPa and, even at 800 °C, the UTS was still 1700 MPa. For the thicker foils, an earlier onset and a more pronounced hardening could be observed. Already for the 300 µm foil, the UTS dropped below 2000 MPa at room temperature. Apart from the hardening and the overall strength, the flat plateau, where the 100 µm foil ran out after hardening at nearly all the tested temperatures, distinguished the curve shape of the 100 µm foil from all the other tested specimens. This puzzling phenomenon was previously mentioned by Wei et al. [11]. These plateaus represent an ongoing plastic

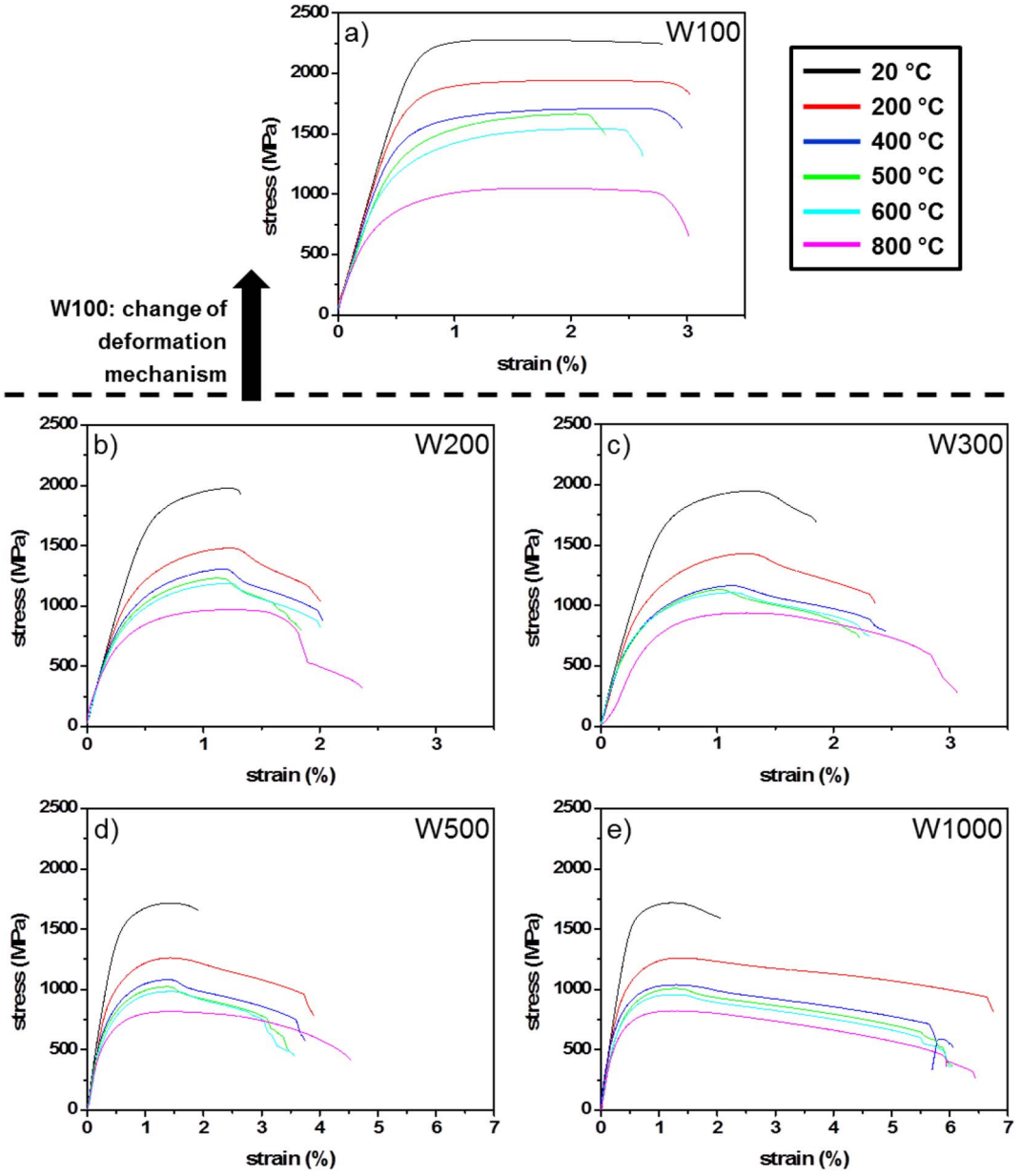

Fig. 2. Engineering stress-strain curves from tensile experiments conducted on the 100 µm (a), 200 µm (b), 300 µm (c), 500 µm (d) and 1000 µm (e) foils. All sheets were tested in the temperature range from 20 °C to 800 °C (curve colour code).

deformation without hardening, even at room temperature. One possible explanation could be a balancing of nucleation and annihilation of dislocations at the increased number of grain boundaries. However, the annihilation of dislocations at grain boundaries is less likely to occur at low homologous temperatures. A second hypothesis is an ordered glide of screw dislocations along high angle grain boundary channels formed by the pancake-shaped, thin grains (pancake grain shape and increased number of HAGBs in 100 µm foil: see [30]). This ordered dislocation glide could prevent work hardening by allowing very few glide systems and thereby reducing the formation and cutting of forest dislocations.

This hypothesis finds support in similar studies. Reiser et al. [36] showed that cold rolled molybdenum behaves very similarly to cold-rolled tungsten, which also forms a plateau in the stress-strain curve under tensile load at room temperature. In comparison, heavily deformed tungsten wires, which do not possess the pancake-shaped grains due to the wire drawing process, show stress-strain curves without plateau formation [37]. We conclude that not just the overall grain size is important for the observed changes in the deformation mechanism, but that the grain shape achieved by severe rolling of the material is also necessary for this peculiar behaviour to occur.

Furthermore, the 200 µm to 500 µm foils and, to a lower degree, the 1 mm plate showed a peculiar yield phenomenon after reaching their ultimate tensile strength. This yield phenomenon in the stress-strain curve is similar to an observation in single crystalline tungsten pulled along the ⟨110⟩ direction [24]. Considering that our tensile tests were performed along the rolling direction and the cold rolled tungsten possessed the highest intensities at the (001) ⟨110⟩ -texture ([30]), the strongly textured material seems to behave like the single crystal material. However, the 100 µm foil, which was even more severely textured, did not show this phenomenon. The same behaviour can be found in Reiser et al. [35], who showed how the yield phenomenon vanishes with a finer microstructure for specimens with the same thickness. The cause of this yield phenomenon and its vanishing at a UFG microstructure remains uncertain.

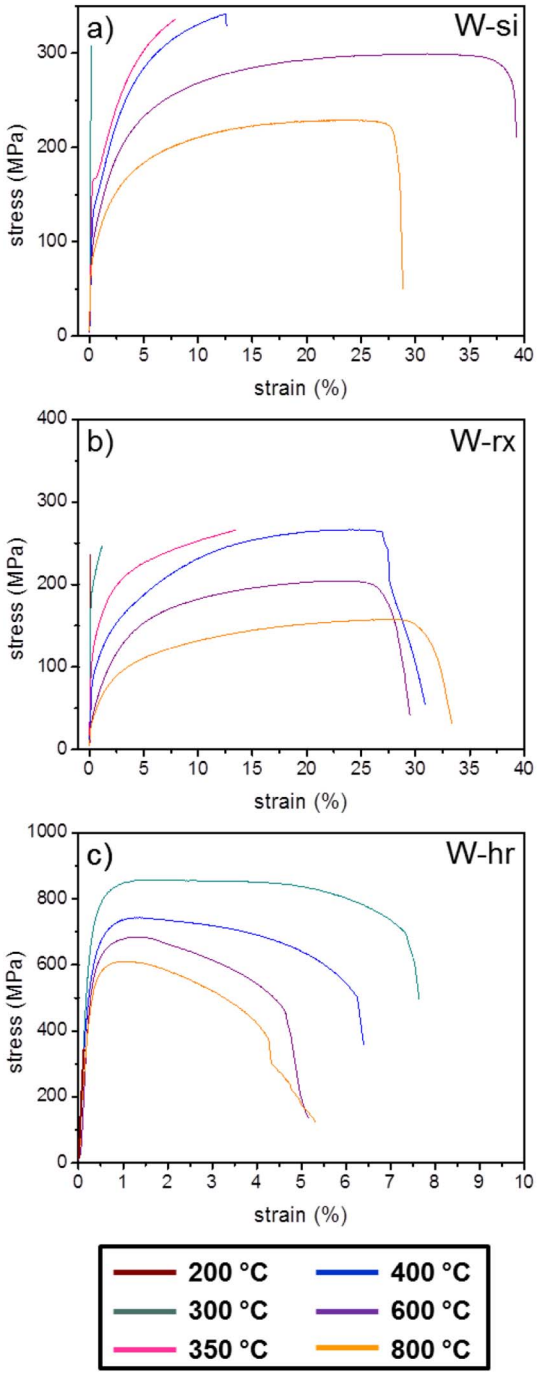

Fig. 3. Engineering stress-strain curves from tensile experiments conducted on the reference materials: sintered tungsten (W-si, a), recrystallized tungsten (W-rx, b) and hot rolled tungsten (W-hr, c). All sheets were tested in the temperature range from 200 °C to 800 °C (curve colour code).

3.2. Flow stress

From the stress-strain curves in Figs. 2 and 3, the flow stress necessary for a plastic strain of 0.2% in the loading direction can be determined as a common characteristic value for the strength of a material. For this purpose, the elastic region of each curve was fitted and the stress at 0.2% plastic strain was calculated. The flow stresses for the five cold rolled sheets, as well as for the recrystallized, coarse-grained tungsten, are plotted in Fig. 4(a) over a temperature range from − 50 °C to 800 °C. The values for temperatures below room temperature were obtained using a similar setup on a Zwick1474 with nitrogen cooling.

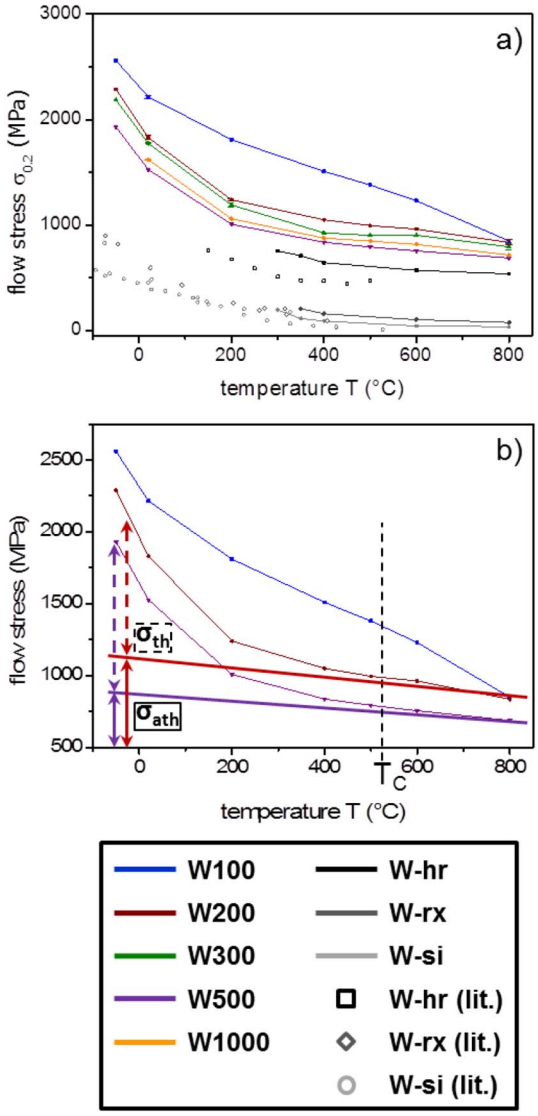

Fig. 4. a: Flow stress at 0.2% plastic strain against the temperatures (T) ranging from − 50 °C to 800 °C for different sheets. b: Splitting of the flow stress into an athermal part (σ_{ath}, continuous line) and a thermal part (σ_{th}, dashed line) by fitting the asymptotic behaviour at temperatures above T_c. No such split is possible for the 100 µm foil. (For interpretation of the references to colour in this figure, the reader is referred to the web version of this article.)

Specimens that showed brittle fracture before reaching 0.2% plastic deformation were not included in Fig. 4. The graph is complemented by the flow stresses found in literature (Fig. 1).

Fig. 4(a) shows a clear trend for the flow stress of the different tungsten samples: two reference materials, W-rx and W-si, exhibited very low flow stresses with a slight increase in the flow stress at lower temperatures, which is comparable to results found in literature. In hot rolled tungsten, the flow stresses are already increased by around 500 MPa. The cold rolled tungsten plates with a thickness between 1 mm (W1000) and 200 µm (W200) all exhibited similar flow stresses with a trend of increased flow stress with an increased degree of deformation. The 100 µm foil distinguishes itself from the other cold rolled plates by an even more enhanced flow stress for temperatures up to 600 °C and a peculiar drop at higher temperatures. This significant increase in the flow stress can be attributed to the fine grain structure and cold-work-induced defects introduced by the (cold) rolling process.

All specimens showed a decreasing flow stress with increasing temperature and then flattened of asymptotically at higher temperatures. Only the flow stress of the 100 µm foils decreased linear and did

not show the asymptotic behaviour up to 800 °C. From this behaviour, a first hint towards the evolution of the deformation mechanism can be deduced. Fig. 4(b) shows that, by fitting the asymptotic progression, the flow stress can be split into an athermal part (σ_{ath}) and a thermal part (σ_{th}). The athermal part can be attributed to the microstructure forming obstacles to the dislocation motion, while the thermal part results from the necessary activation of screw dislocations at temperatures beneath the critical temperature (T_c) [38,39]. Fig. 4(b) illustrates the evolution of these parts from the 500 µm foil (purple) to the more heavily deformed, 200 µm foil (red). The athermal part increases as expected, which can be attributed to the grain refinement and the increase of lattice defects from cold rolling. The thermal part, however, remains constant, which indicates that the same additional energy for the activation of the screw dislocations is necessary. Therefore, no change in the dominant deformation mechanism is expected.

Compared to the asymptotic behaviour of the 200 µm to 1 mm sheets, as well as the reference materials, the 100 µm sheet showed not only a strongly increased flow stress, but it also showed a nearly linear decrease in the flow stress upon increasing temperature to 800 °C. Notably, it did not display asymptotic behaviour, which can possibly be attributed to recovery effects at elevated temperatures. The 100 µm foil, as the foil with the highest degree of deformation and smallest grain size, possess supposedly a microstructure far from thermal equilibrium. Even though the common approach of splitting the flow stress, as demonstrated, cannot be applied here and the usual interpretation fails, the steady decrease over temperature range indicates that the screw dislocation still plays an important role in the deformation behaviour of UFG tungsten.

In Fig. 5, the flow stress is correlated to the grain size derived from the EBSD measurements [30], which is done to investigate the strengthening behaviour based on the Hall-Petch relation. By plotting the flow stress over the square root of the inverse grain size for different temperatures and performing a linear fit for each temperature, the slope of the regression lines corresponded to their respective Hall-Petch coefficient, k_P, following Eq. (1). The upper x-axis shows the sheet thickness corresponding to the grain size in the lower x-axis.

The following discussion, which is based on the results of this plot, must be treated with care, because the discussion of flow stress (σ) over grain size is more about a discussion of flow stress over microstructure, where the grain size (d), as the main microstructural parameter, is altered by the increased degree of deformation. There could be other contributing factors to the flow stress being altered by cold rolling. Examples include the dislocation density, texture and the nature of the grain boundaries, but these factors are hard to quantify. For a simplified examination, these contributions are considered constant for the differently thick sheets and are represented by σ_0.

$$\sigma = \sigma_0 + k_P \cdot d^{-1/2} \quad (1)$$

The positive slope of all Hall-Petch coefficients shows that the grain size has a positive effect on the strengthening behaviour. This even occurs at an elevated temperature of 800 °C. However, k_P also exhibits a strong temperature dependence, where the trend shows a decrease of k_P with increasing temperature, except between 20 °C and 200 °C. This trend fits the simulated results from Ahmed and Hartmaier [40] for UFG material. Ahmed and Hartmaier demonstrated that UFG materials tend to show a strong dependency of the Hall-Petch constant on temperature, which they based on a model of the grain-boundary-mediated plasticity: when approaching a grain boundary, dislocations can be either blocked by it, which leads to a dislocation pile up, or the dislocations can be absorbed by the grain boundary. When being absorbed, the model by Ahmed and Hartmaier proposes a split of the Burgers vector into two components, which forms a grain boundary glide dislocation and a grain boundary climb dislocation. These new dislocations can move away from the interaction point and reduce the pile up. Given that the grain boundary climb dislocation moves by climbing within the grain boundary, which is a diffusion-triggered process, the grain-boundary-mediated mechanism gains influence with increasing temperature. This change in deformation mechanism – from blocking to absorbing grain boundaries – could account for the observed decrease in the Hall-Petch constant, which shows that the flow stress is less dependent on the grain size at higher temperatures.

A similar behaviour was found by Reiser et al. [36], who showed that, for UFG tungsten, the grain shape effect of the tensile anisotropy (different tensile behaviours when testing 0° or 90° to the rolling direction) vanishes at temperatures above 600 °C.

3.3. Uniform elongation

Additional important parameters regarding ductility, which can be extracted from the stress-strain curves, are the uniform elongation (ε_{ue}) and the elongation at failure (ε_{ef}). As mentioned in Section 1, ε_{ue} is the more reliable value when testing samples with different thickness, because there exists only a small trend to a decreasing uniform elongation for thinner specimens [23,41]. In this work, we use the definition of uniform elongation as the plastic strain at the ultimate tensile strength. The temperature dependence of the uniform elongation for the five different, cold rolled sheets, as well as for the three reference materials, is plotted in Fig. 6. To accommodate the broad range of values for ε_{ue} at

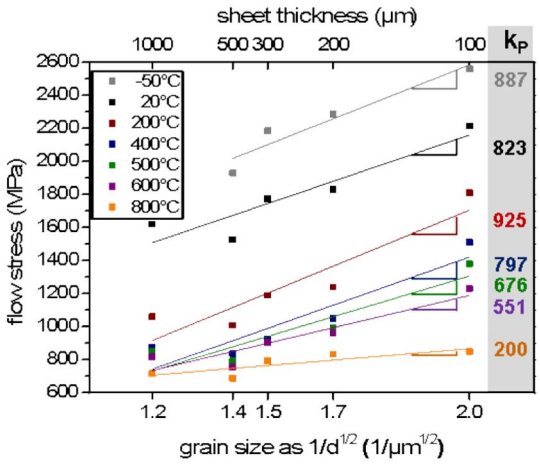

Fig. 5. Flow stress against the grain size as $d^{-1/2}$ (lower x-axis, linearly scaled) and the respective sheet thicknesses (upper x-axis). The data set for each temperature was fitted linearly following the Hall-Petch relation, where the respective Hall-Petch coefficients (slope [MPa/µm$^{-1/2}$]) are given.

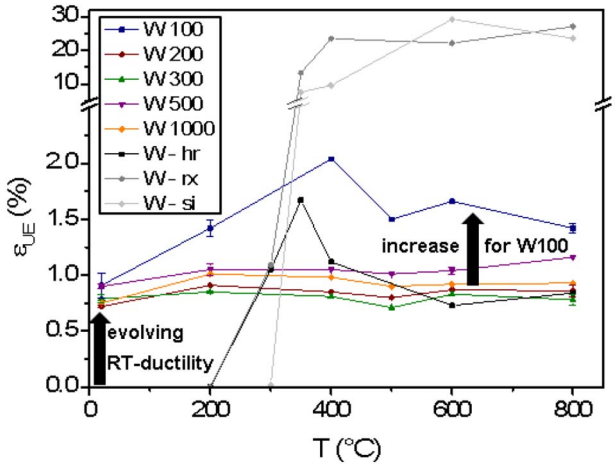

Fig. 6. Uniform elongation (ε_{ue}) against temperature (T) for five different, cold rolled sheets and three reference materials. ε_{ue} was extracted from the tensile curves in Figs. 2 and 3 at the plastic strain for their respective UTSs.

high temperatures, the y-axis is broken into two parts with different scalings.

The uniform elongation over the sheet thickness, respective to the microstructure, shows some clear tendencies. The recrystallized tungsten and the sintered compact – the two materials that did not experience any severe deformation directly prior to testing – exhibited uniform elongations of 15 to 30% at temperatures above 400 °C. In comparison, the warm rolled and the cold rolled specimens showed a low uniform elongation with values ranging largely between 0.7 and 2% plastic strain. There was no clear correlation between the grain size and the uniform elongation for the rolled specimens. Only the 100 µm foil stands out with values of around 1.5 to 2%. However, while the three reference materials all lost their ductility at around 300 °C, the cold rolled sheets maintained their ductility down to at least room temperature. Neither the residual ductility for the cold rolled specimen at low temperatures, nor the increased ductility of the 100 µm foil should be a measuring artifact, because the uniform elongation is mainly independent of specimen thickness. The very thin specimen should, if at all, experience a decrease in its uniform elongation due to the decreased thickness [23,41].

The large difference in ε_{ue} for high temperatures could be expected from the classical picture of lower free path lengths for dislocations in large grains and a faster pile-up at grain boundaries for the much finer grained material. However, preservation of some residual ductility at low temperatures for the cold rolled material and the significant increase in ductility for the W100 foil do not fit this picture. Additional mechanisms supporting plastic deformation must be active, but the authors can only speculate at the moment. It is possible that a fine-grained specimen could exhibit a significantly increased amount of dislocation nucleation sites, which could allow for their room temperature ductility. A dominance of dislocation nucleation also fits the temperature independence of ε_{ue} for the cold rolled material. Further, the mechanism of confined plastic slip in this pancake-like structure, as mentioned in Section 3.1, may provide a possible explanation for the plateau formation in the stress-strain curves by offering an undisturbed dislocation motion. This is especially true for the 100 µm foil because of its UFG microstructure.

3.4. Hardening behaviour

Observations of the stress-strain curves in Section 3.1 allow for a qualitative interpretation of possible changes in the hardening behaviour. To support these observations quantitatively, it is necessary to calculate the hardening coefficients for the different microstructures and temperatures. This calculation requires fitting the true stress-true strain curve and the derivation of the slope of each curve at every point. This slope is called the “hardening coefficient”, where $\theta = d\sigma/d\varepsilon$ and gives an impression of the strain hardening rate over the progressive strain. In literature, there are various models to fit the stress-strain curve, which are obtained from tensile tests. They range from simple fits, such as the ones used by Holloman [42] and Voce [43], to the advanced “generalized Voce fit” used by Tome et al. [44] (see Eq. (2)) or to the fit used by Chinh et al. [45] (see Eq. (3)). These later two models use an exponential power law as the basis for the constitutive relationship between stress and strain, which usually covers the region between the elastic limit (up to which the hardening coefficient corresponds to the Young's modulus) and the ultimate tensile strength (UTS).

The “generalized Voce fit” links stress (σ) and strain (ε) according to:

$$\sigma = \sigma_0 - (\sigma_1 + \theta_1\varepsilon)[1 - exp(-\theta_0\varepsilon/\sigma_1)] \quad (2)$$

where σ_0 is the stress, θ_0 is the slope at $\varepsilon = 0$ and σ_1 and θ_1 are additional fit parameters.

However, the model used by Tome does not give much scope for fitting large differences in hardening behaviour due to the limited variability of the coefficients in the exponent.

Chinh et al. tried to solve this problem by incorporating an additional exponent as follows:

$$\sigma = \sigma_0 + \sigma_1[1 - exp(-\varepsilon^n/\varepsilon_c)] \quad (3)$$

where σ_0 is the stress at $\varepsilon = 0$, $(\sigma_1 + \sigma_0)$ is the saturation stress and n and ε_c are further fit constants that help to fit metals over a wide range of strains, including those for ECAP-processed materials. This equation, however, entails a fit starting with a slope of 0 at $\sigma = \sigma_0$ and ends in a horizontal line for large strains.

Due to these deficiencies, neither of these models allows a sufficient fit of the versatile tensile behaviour of the severely deformed tungsten sheets tested in this work. Here, we propose a new model to fit the hardening region of a large variety of stress-strain curves by combining the models of Tome and Chinh (see Eq. (4)):

$$\sigma = \sigma_0 + (\sigma_1 + \theta_1\varepsilon)[1 - exp(-\theta_2\varepsilon^n)] + \sigma_2[1 - exp(-E\varepsilon/\sigma_2)] \quad (4)$$

In this fit, σ_0 represents the flow stress (at $\varepsilon = 0$), σ_1 and σ_2 are fit parameters that influence the UTS, θ_1 is the slope for large strains and θ_2 and n are additional free fit parameters. Finally, the equation allows us to provide the correct slope at the beginning of the fit in the form of the Young's modulus E.

The peculiar hardening behaviour observed for the 100 µm foil, which presents itself as a nearly elastic-perfectly-plastic behaviour, was already mentioned in the discussion of the stress-strain curves (Section 3.1, Fig. 2). This qualitative analysis shall be supported by the calculation of the hardening coefficients for the different tensile tests using Eq. (4). The required true stress-true strain curves are calculated based on the elongation/strain measured by the extensometer: $\varepsilon_{true} = \ln(1 + \varepsilon_{eng})$ and $\sigma_{true} = \sigma_{eng}(1 + \varepsilon_{eng})$ [46]. The evaluation is performed between the elastic limit (end of constant slope) and the ultimate tensile strength, because the approach of true stress fails after reaching the UTS due to a locally diminishing cross section through necking.

Fig. 7 shows exemplarily the plastic region and the fit of this region of the tensile curves for three extreme conditions: the 100 µm foil at room temperature, as well as the 500 µm sheet and the hot rolled tungsten sheet tested at 800 °C. Even though these curves show a highly differing progression, they can be fitted successfully by the equation developed in this paper (Eq. (4)). The fits are represented as red curves in Fig. 7. Both fits exhibit coefficients of determination (R^2) above 0.99 (W100, 20 °C: 0.9998; W-hr, 800 °C: 0.9981), which indicates successful fits.

From fitting the individual curves, the derivative for each strain can be calculated. This derivative is called the hardening coefficient and is plotted for the tensile tests at 20 °C and 800 °C against the plastic strain for three representative sheets (W100, W200, W500) and a hot rolled plate as a reference material (W-hr). The hardening coefficient for the hot rolled plate at room temperature can't be determined by tensile tests due to the brittle fracture of this coarse-grained tungsten occurring below 300 °C. At 20 °C (Fig. 7b), the cold rolled sheets showed a different hardening behaviour. The 500 µm sheet exhibited the slowest hardening rate (upmost curve) and the 200 µm sheet was a little beneath it. The 100 µm foil, however, showed a much faster hardening, reaching nearly $\theta = 0$ (plateau) at 0.5% plastic strain. But then it showed greater deformation than the two thicker specimens. At 800 °C (Fig. 7c), these differences in hardening behaviour, which were obtained through cold rolling, nearly vanish entirely. Compared to coarse-grained tungsten (W-hr), the cold rolled plates all show a slower hardening rate at elevated temperatures.

These hardening curves transfer the qualitative impression, as gained from Fig. 2, to quantitative and analysable values. The fast hardening of the 100 µm foil at room temperature and the long residual plastic strain without hardening, support the proposed changes in the deformation mechanism between foils with a degree of deformation of 3.3 (200 µm foil) and foils with a degree of deformation of 4 (100 µm foil).

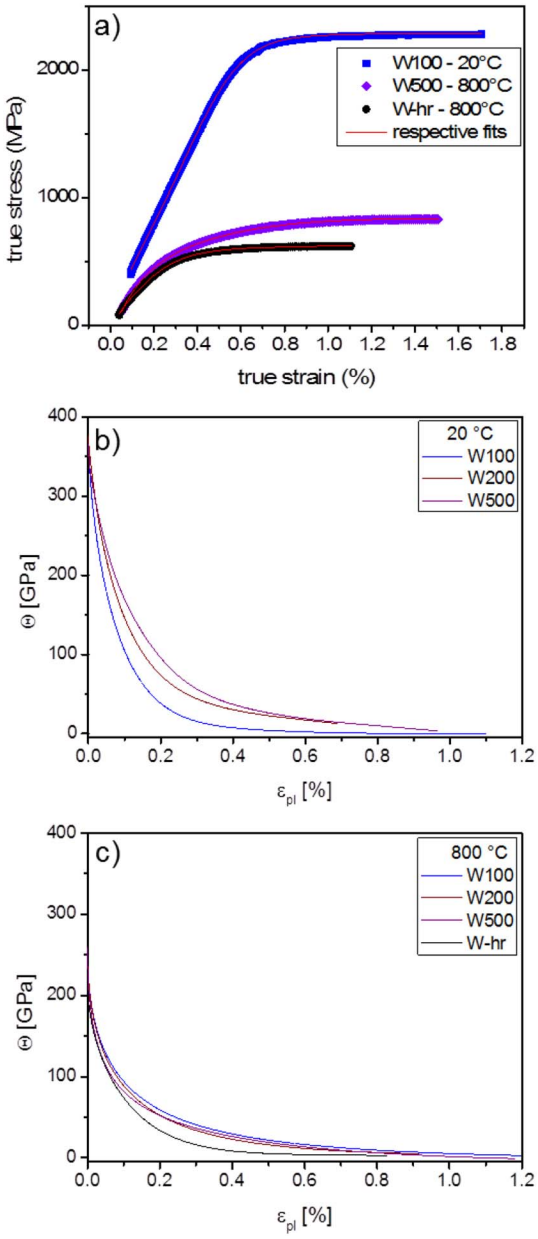

Fig. 7. a) True stress-true strain curve for: the 100 µm foil (W100) tested at 20 °C (blue), the 500 µm foil (W500) tested at 800 °C (purple) and a hot rolled reference specimen (W-hr) tested at 800 °C (black). The red lines indicate the respective fits of the two curves based on Eq. (4), which starts at $\varepsilon_{pl} = 0$. The bottom rows show hardening coefficients θ for 20 °C (b) and 800 °C (c) for W100, W200, W500 and W-hr. (For interpretation of the references to colour in this figure legend, the reader is referred to the web version of this article.)

3.5. Fractography

An SEM analysis of representative sample's fracture surfaces is depicted in Fig. 8. All analyzed fractures occurred during the tensile tests shown in Figs. 2 and 3. The low magnification SEM micrographs were obtained using the secondary electron detector of a Zeiss Merlin SEM. The series at 20 °C (Fig. 8a) shows one exemplary fracture surface of each of the five different sheets, tested at 20 °C. The W100 series (Fig. 8b) compares the fracture behaviour over the tested range of temperatures for the 100 µm foil.

Fig. 8(a) shows that, while the 1000 µm and the 500 µm foils exhibited a solely brittle fracture surface, the fracture mechanisms for the 300 µm foil started to change towards a lamellar fracture. For the 300 µm and the 200 µm foils, there existed a lamellar region stretching from one edge of the foil to over nearly one quarter of the fracture's length. The remaining part of the fracture surfaces showed a brittle fracture. The failure mechanism was supposedly a crack that started at the edge with the lamellar structure and propagated steadily by means of lamellar formation until the stress in the remaining cross section exceeded the critical crack length. This resulted in a brittle residual fracture. The lamellar region in the 200 µm foils increased slightly compared to the 300 µm foil, but only the 100 µm foil exhibited a lamellar fracture over the entire cross-sectional area without any hint of brittle fracture.

The series at 20 °C shows that, by a mere alteration of the microstructure towards ultrafine-grain sizes, the fracture behaviour can be manipulated towards a tough fracture with lamellar formation. These results fit the fracture analysis of Wei et al. [11], who also found lamellar fractures after tensile tests with low temperature rolled tungsten.

The 100 µm foil exhibited the most interesting mechanical properties and a full lamellar fracture at room temperature. The fracture surface was analyzed for several temperatures ranging from room temperature to 800 °C (see Fig. 8b). It is qualitatively observable, that the 100 µm foil showed the highest number of single lamellas at room temperature and that the number of lamellas decreased with increasing temperature. For the 800 °C specimen only, the fracture surface looked distinctly different and showed the more “usual” tough fracture instead of a lamellar fracture.

A lamellar fracture at low homologous temperatures for the highly deformed foils (Fig. 8a and b) may lead to the conclusion that there is no evolving room temperature ductility in the classical sense, i.e. glide of dislocations, as suggested by the tensile test results. It rather hints to the fact that other inelastic mechanisms could be responsible for the measured elongation. One such mechanism could be microcracking, as other typical mechanisms like adiabatic shear band formation or twin formation won't take place at the applied low strain rates and high testing temperatures. However, the two side views of the fracture plane of a 100 µm foil tested at room temperature showed distinct necking towards the fracture plane. This does not exclude the possibility that other inelastic mechanisms play a role, but it does prove that plastic deformation due to dislocation motion takes place during tensile tests.

4. Conclusions

In this work, the tensile properties of cold rolled tungsten and their dependence on the microstructure were investigated by studying plates with different thicknesses ranging from 1 mm to 100 µm. These fine- and ultrafine-grained plates were compared to coarser grained reference materials. This detailed analysis is important for shedding light onto the deformation mechanisms in UFG tungsten and to gain an understanding of the reasons for the improved mechanical properties found in UFG tungsten foils.

Referring to the main questions stated in the Introduction (Section 1), we can conclude the following:

(1) While the reference materials showed brittle fractures under a tensile load below 300 °C, the cold rolled tungsten exhibited room temperature ductility and simultaneously reached higher stresses. The tensile curves for the 100 µm foil stood out due to plateau formation after hardening for all investigated temperatures up to 800 °C.
(2) Cold rolling leads to a steady increase in the flow stress, which can be attributed to the increased number of obstacles formed by grain refinement and cold-rolled-induced lattice defects. The temperature dependence of the flow stress, its asymptotic behaviour at higher temperatures and the constant thermal part of the flow stress for the reference and cold rolled sheets all indicate that the screw dislocations still control the plastic deformation. Despite an increased flow stress and still-active screw dislocations, cold rolled tungsten

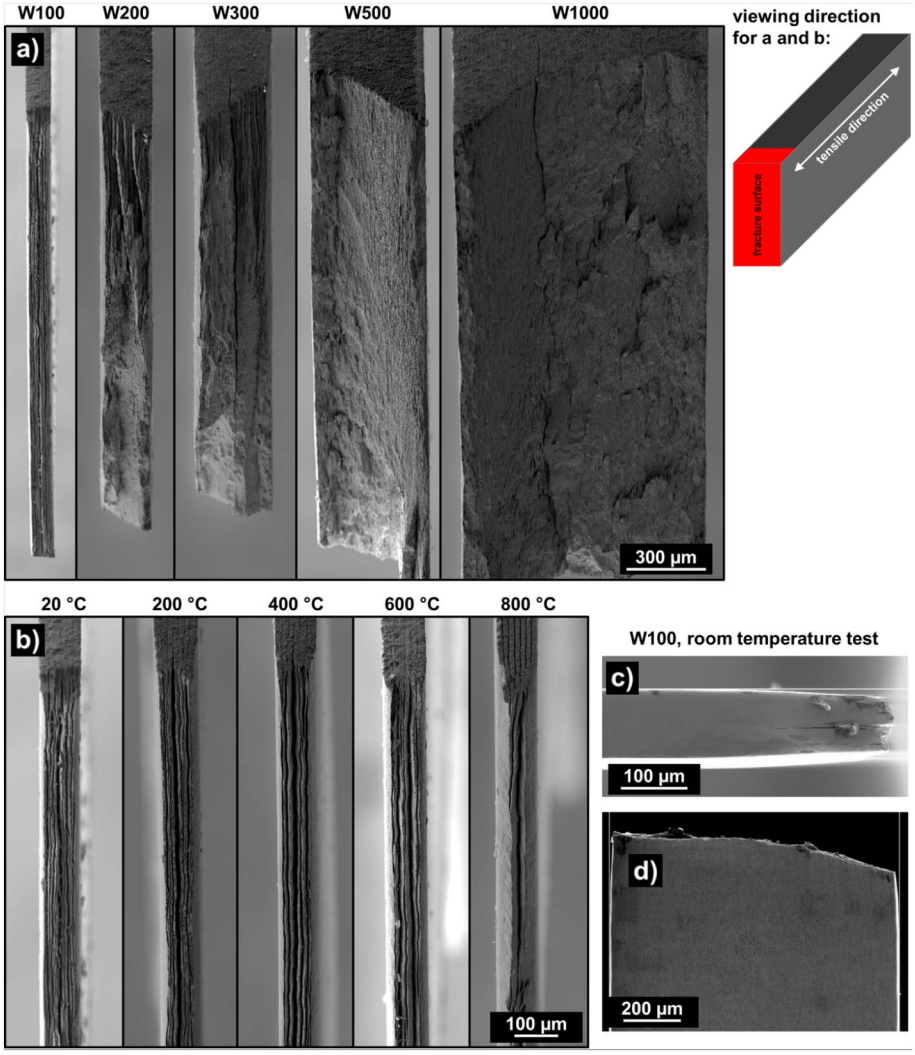

Fig. 8. Fracture surfaces of cold rolled tungsten sheets and foils with different thicknesses for room temperature tests (a) and of the 100 µm foil at temperatures from 20 °C to 800 °C (b). The viewing direction of the SEM images is depicted in the top right corner. Figs. (c) and (d) show both side views of a 100 µm tensile specimen after testing and the necking closest to the fracture plane.

foils also exhibited uniform elongation of around 1% at room temperature. The 100 µm foil had the highest flow stress and the largest uniform elongation among all the cold rolled tungsten sheets at all tested temperatures.

(3) The fracture surface of each specimen tested at room temperature showed that, by altering the microstructure towards ultrafine-grain sizes, the fracture behaviour can change from a brittle fracture towards a lamellar fracture. The necking of the sample clearly indicated that plastic deformation, in terms of a dislocation glide, takes place. The 100 µm foil breaks entirely by lamellar formation. By increasing the testing temperature, the number of lamellas decreases in favor of a more classic ductile fracture.

(4) From the discussed results, initial conclusions can be drawn regarding the mechanisms controlling the plastic deformation: the temperature dependence of the flow stresses shows that the screw dislocations are still dominant in the UFG regime. However, cold rolling also led to evolving room-temperature ductility, which may be caused by cold-rolling-induced dislocation nucleation sites. From the stress-strain curves shown in Fig. 2, we infer that a change in the deformation mechanism takes place when rolling from a deformation degree of 3.3 (200 µm foil, grain size: 360 nm in the S-direction) to a deformation degree of 4 (100 µm foil, grain size: 240 nm in the S-direction). The plateau formation and, hence, the hardening free region of the 100 µm tensile curves suggests that the dislocations can glide without interaction among each other within the channels formed by the small grains. Finally, from the decreasing Hall-Petch coefficients obtained at elevated temperatures, it can be derived that a change in the dislocation-grain-boundary interactions takes place. A change from blocking, at low temperatures, to absorbing, at elevated temperatures, is postulated.

Based on these results, it can be concluded that the cold rolling of commercial pure tungsten has a positive influence on many important mechanical properties. The combination of increased strength and the simultaneous evolution of room-temperature ductility for UFG tungsten promises technical applicability and interesting further studies on the underlying deformation mechanisms. Considering that, even for the smallest investigated microstructure, no saturation was visible for increasing flow stresses and uniform elongations, there seems to be additional potential if higher degrees of deformation are realized.

Acknowledgements

The authors gratefully acknowledge funding of this work by the Deutsche Forschungsgemeinschaft under Grant No. RE3551/2-1. The support of the tungsten supplier, PLANSEE SE, Reutte/Austria, is gratefully acknowledged. Special thanks go to Siegfried Baumgärtner for the support during the mechanical testing.

References

[1] G.A. Geach, J.E. Hughes, The alloy of rhenium with molybdenum or with tungsten

and having good high temperature properties, Proceedings of 2nd Plansee Seminar, Plansee AG, Reutte, 1955, p. 245.
[2] A. Luo, D.L. Jacobson, K.S. Shin, Solution softening mechanism of iridium and rhenium in tungsten at room temperature, Int. J. Refract. Met. Hard Mater. 10 (1991) 107–114.
[3] P.L. Raffo, Yielding and fracture in tungsten and tungsten-rhenium alloys, J. Less-Common Met. 17 (1969) 133–149.
[4] J. Du, T. Höschen, M. Rasinski, J.-H. You, Interfacial fracture behavior of tungsten wire/tungsten matrix composites with copper-coated interfaces, Mater. Sci. Eng. A 527 (2010) 1623–1629.
[5] J. Riesch, J.-Y. Buffiere, T. Höschen, M. Di Michiel, M. Scheel, C. Linsmeier, J.-H. You, In situ synchrotron tomography estimation of toughening effect by semi-ductile fibre reinforcement in a tungsten-fibre-reinforced tungsten composite system, Acta Mater. 61 (2013) 7060–7071.
[6] R.Z. Valiev, Y. Estrin, Z. Horita, T. Langdon, M.J. Zehetbauer, Y. Zhu, Producing bulk ultrafine-grained materials by severe plastic deformation, JOM 4 (2006) 33–39.
[7] Q. Wei, T. Jiao, K. Ramesh, E. Ma, L. Kecskes, L. Magness, R. Dowding, V. Kazykhanov, R. Valiev, Mechanical behavior and dynamic failure of high-strength ultrafine grained tungsten under uniaxial compression, Acta Mater. 54 (2006) 77–87.
[8] T. Hao, Z.Q. Fan, S.X. Zhao, G.N. Luo, C.S. Liu, Q.F. Fang, Microstructures and properties of ultrafine-grained tungsten produced by equal-channel angular pressing at low temperatures, J. Nucl. Mater. 1-3 (2013) 351–356.
[9] M. Faleschini, H. Kreuzer, D. Kiener, R. Pippan, Fracture toughness investigations of tungsten alloys and SPD tungsten alloys, J. Nucl. Mater. 367-370 (2007) 800–805.
[10] Q. Wei, H. ZHANG, B. SCHUSTER, K. Ramesh, R. Valiev, L. Kecskes, R. Dowding, L. Magness, K. CHO, Microstructure and mechanical properties of super-strong nanocrystalline tungsten processed by high-pressure torsion, Acta Mater. 54 (2006) 4079–4089.
[11] Q. Wei, L.J. Kecskes, Effect of low-temperature rolling on the tensile behavior of commercially pure tungsten, Mater. Sci. Eng. A 491 (2008) 62–69.
[12] Q. Wei, L.J. Kecskes, K.T. Ramesh, Effect of low-temperature rolling on the propensity to adiabatic shear banding of commercial purity tungsten, Mater. Sci. Eng. A 578 (2013) 394–401.
[13] J. Reiser, M. Rieth, B. Dafferner, A. Hoffmann, X. Yi, D.E.J. Armstrong, Tungsten foil laminate for structural divertor applications – analyses and characterisation of tungsten foil, J. Nucl. Mater. 1-3 (2012) 197–203.
[14] E.O. Hall, The deformation and ageing of mild steel, Proc. Phys. Soc. B 64 (1951) 747–753.
[15] N.J. Petch, The cleavage strength of polycrystals, J. Iron Steel Inst. 174 (1953) 25–28.
[16] R.Z. Valiev, I.V. Alexandrov, Y.T. Zhu, T.C. Lowe, Paradox of strength and ductility in metals processed bysevere plastic deformation, J. Mater. Res. 17 (2002) 5–8.
[17] I.V. Aleksandrov, G.I. Raab, L.O. Shestakova, A.R. Kil'mametov, R.Z. Valiev, Refinement of tungsten microstructure by severe plastic deformation, Phys. Met. Metallogr. 93 (2002) 493–500.
[18] L.J. Kecskes, K.C. Cho, R.J. Dowding, B.E. Schuster, R.Z. Valiev, Q. Wei, Grain size engineering of bcc refractory metals: top-down and bottom-up—application to tungsten, Mater. Sci. Eng. A 467 (2007) 33–43.
[19] J. Reiser, S. Wurster, J. Hoffmann, S. Bonk, C. Bonnekoh, D. Kiener, R. Pippan, A. Hoffmann, M. Rieth, Ductilisation of tungsten (W) through cold-rolling: r-curve behaviour, Int. J. Refract. Met. Hard Mater. 58 (2016) 22–33.
[20] V. Nikolic, S. Wurster, D. Firneis, R. Pippan, Improved fracture behavior and microstructural characterization of thin tungsten foils, Nucl. Mater. Energy 9 (2016) 181–188.
[21] J. Reiser, J. Hoffmann, U. Jäntsch, M. Klimenkov, S. Bonk, C. Bonnekoh, M. Rieth, A. Hoffmann, T. Mrotzek, Ductilisation of tungsten (W): on the shift of the brittle-to-ductile transition (BDT) to lower temperatures through cold rolling, Int. J. Refract. Met. Hard Mater. 54 (2016) 351–369.
[22] A. Németh, J. Reiser, D.E.J. Armstrong, M. Rieth, The nature of the brittle-to-ductile transition of ultra fine grained tungsten (W) foil, Int. J. Refract. Met. Hard Mater. 50 (2015) 9–15.
[23] Y.H. Zhao, Y.Z. Guo, Q. Wei, T.D. Topping, A.M. Dangelewicz, Y.T. Zhu, T.G. Langdon, E.J. Lavernia, Influence of specimen dimensions and strain measurement methods on tensile stress–strain curves, Mater. Sci. Eng. A 525 (2009) 68–77.
[24] A.S. Argon, S.R. Maloof, Plastic deformation of tungsten singel crystals at low temperatures, Acta Metall. 14 (1966) 1449–1462.
[25] J.W. Christian, Some surprising features of the plastic deformation of body-centered cubic metals and alloys, Metall. Trans. A. 14 (1983) 1237–1256.
[26] V. Vitek, F. Kroupa, Dislocation theory of slip geometry and temperature dependence of flow stress in B.C.C. metals, Phys. Status Solidi B 18 (1966) 703–713.
[27] V. Vítek, Thermally activated motion of screw dislocations in B.C.C. metals, Phys. Status Solidi B 18 (1966) 687–701.
[28] P.B. Hirsch, Acta Cryst 13 (1960) 1114.
[29] B. Sestak, A. Seeger, Gleitung und Verfestigung in kubisch raumzentrierten Metallen und Legierungen (II), Z. Metallkd. 69 (1978) 355–363.
[30] S. Bonk, J. Reiser, J. Hoffmann, A. Hoffmann, Cold rolled tungsten (W) plates and foils: evolution of the microstructure, Int. J. Refract. Met. Hard Mater. 60 (2016) 92–98.
[31] D. Brunner, Comparison of flow-stress measurements on high-purity tungsten single crystals with the kink-pair theory, Mater. Trans. JIM 41 (2000) 152–160.
[32] H. Schultz, Defect-sensitive properties of tungsten and other bcc transition metals, Z. Metallkd. 78 (1987) 469–477.
[33] T. Shen, Y. Dai, Y. Lee, Microstructure and tensile properties of tungsten at elevated temperatures, J. Nucl. Mater. 468 (2016) 348–354.
[34] D. Cereceda, M. Diehl, F. Roters, D. Raabe, J. Manuel Perlado, J. Marian, Unraveling the temperature dependence of the yield strength in single-crystal tungsten using atomistically-informed crystal plasticity calculations, Int. J. Plast. (2016) 242–265.
[35] J. Reiser, J. Hoffmann, U. Jäntsch, M. Klimenkov, S. Bonk, C. Bonnekoh, A. Hoffmann, T. Mrotzek, M. Rieth, Ductilisation of tungsten (W): on the increase of strength and room-temperature tensile ductility through cold-rolling, Int. J. Refract. Met. Hard Mater. (2016).
[36] J. Reiser, M. Rieth, A. Moeslang, B. Dafferner, A. Hoffmann, X. Yi, D. Armstrong, Tungsten foil laminate for structural divertor applications - tensile test properties of tungsten foil, J. Nucl. Mater. 434 (2013) 357–366.
[37] D. Terentyev, J. Riesch, S. Lebediev, A. Bakaeva, J.W. Coenen, Mechanical properties of as-fabricated and 2300 °C annealed tungsten wire tested up to 600 °C, Int. J. Refract. Met. Hard Mater. 66 (2017) 127–134.
[38] A. Seeger, Theorie der Kristallplastizität, Z. Naturforsch. 9a (1954) 870–881.
[39] V. Schulze, O. Vöhringer, Influence of alloying elements on the strain rate and temperature dependence of the flow stress of steels, Metall. Mater. Trans. A 31A (2000) 825–830.
[40] N. Ahmed, A. Hartmaier, Mechanisms of grain boundary softening and strain-rate sensitivity in deformation of ultrafine-grained metals at high temperatures, Acta Mater. 59 (2011) 4323–4334.
[41] Y. ZHAO, Y. GUO, Q. Wei, A. DANGELEWICZ, C. XU, Y. ZHU, T. LANGDON, Y. ZHOU, E. LAVERNIA, Influence of specimen dimensions on the tensile behavior of ultrafine-grained Cu, Scr. Mater. 59 (2008) 627–630.
[42] J.H. Hollomon, Tensile deformation, Trans. Metall. Soc. AIME 162 (1945) 268–290.
[43] E. Voce, The relationship between stress and strain for homogeneous deformation, J. Inst. Met. 74 (1948) 537–562.
[44] C. Tome, G.R. Canova, U.F. Kocks, N. Christodoulou, J.J. Jonas, The relation between macroscopic and microscopic strain hardening in F.C.C. polycrystals, Acta Mater. 32 (1984) 1637–1653.
[45] N.Q. Chinh, G. Horváth, Z. Horita, T.G. Langdon, A new constitutive relationship for the homogeneous deformation of metals over a wide range of strain, Acta Mater. 52 (2004) 3555–3563.
[46] G. Gottstein, Physical Foundations of Materials Science, 1 ed., Springer-Verlag, Berlin Heidelberg, 2004.